

Degenerate scalar scenario of two Higgs doublet model with a complex singlet scalar

Gi-Chol Cho^{1*} and Chikako Idegawa^{1,2†}

¹ *Department of Physics, Ochanomizu University, Tokyo 112-8610, Japan and*

² *MOE Key Laboratory of TianQin Mission,
TianQin Research Center for Gravitational Physics & School of Physics and Astronomy,
Frontiers Science Center for TianQin,
Gravitational Wave Research Center of CNSA,
Sun Yat-sen University (Zhuhai Campus), Zhuhai 519082, China*

(Dated: January 22, 2025)

Abstract

We study the two Higgs doublet model with a complex singlet scalar whose imaginary part acts as dark matter (DM). The scattering of DM and quarks, mediated by three CP-even scalars in this model, is suppressed when masses of CP-even scalars are degenerate; that is called the “degenerate scalar scenario”. Based on this scenario, we show that the strong first-order electroweak phase transition (EWPT) can be achieved without conflicting with constraints from the DM relic density and the direct detection experiments. We also discuss a shift of scalar trilinear coupling from the Standard Model prediction, which could be a test of this model in collider experiments.

* cho.gichol@ocha.ac.jp

† c.idegawa@hep.phys.ocha.ac.jp, idegawa@mail.sysu.edu.cn

I. INTRODUCTION

Dark matter (DM), whose existence has been suggested by cosmological observations, predicts physics beyond the Standard Model (SM). Among the various DM candidates, weakly interacting massive particles (WIMP) are attractive because their abundance can be explained thermally. It is so-called the “WIMP miracle”. However, despite the vigorous searches, such as accelerator experiments and DM direct detection experiments have not found the DM signal. In particular, the LZ experiment [1] places very strong constraints on the scattering cross sections of WIMP-DM and nucleons, posing a major challenge for models that include WIMP-DM.

Possible scenarios consistent with the current direct detection experiments include (1) DM is either sufficiently massive or has only tiny interactions with the SM particles and (2) DM-nucleon scattering is suppressed by a built-in mechanism in the model. Here, we focus on the second scenario. One model that realizes this scenario is the complex singlet scalar extension of the Standard Model (CxSM) [2], which includes a pseudo Nambu-Goldstone (pNG) DM. In the CxSM, as the name suggests, the SM is extended by adding a complex scalar single particle field S . The imaginary part of S behaves as the pNG DM, whose stability is guaranteed by the CP symmetry of the scalar potential. On the other hand, the real part of S mixes with the SM Higgs boson to form the mass eigenstates h_1 and h_2 . These two particles mediate DM-quark scattering. In ref. [3], the DM-quark scattering is suppressed due to the small momentum transfer. However, this model has a so-called domain wall problem because the Z_2 symmetry ($S \rightarrow -S$) of the scalar potential V is spontaneously broken due to the development of the vacuum expectation value (VEV) of the singlet scalar (S). Therefore, in ref. [4], a linear term of S ($V \supset a_1 S$) that breaks the Z_2 symmetry is introduced, and in this case, it is proposed that when the masses of the two Higgs bosons are degenerate, i.e., $m_{h_1} \simeq m_{h_2}$, this scattering is suppressed. This suppression mechanism is called the degenerate scalar scenario.

On the other hand, baryon asymmetry of the Universe (BAU), along with DM, is one of the unsolved problems. The most testable scenario to realize BAU is electroweak baryogenesis (EWBG) [5–14] associated with the Higgs physics. EWBG requires strong first-order electroweak phase transition (EWPT), which suggests the need for an extension of the SM [15–18]. The CxSM is an attractive model for both DM and BAU, but in ref. [19], the

poor compatibility between the degenerate scalar scenario and strong first-order EWPT. In almost all models, strong first-order EWPT is caused by the effects of the finite temperature and the quantum corrections on the scalar potential, the latter is known as the Coleman-Weinberg potential. However, in some models with extended Higgs sector, the potential barrier is enhanced by mixing between the electroweak Higgs sector and a new scalar sector at the tree level. As investigated in ref. [19], the contribution of the latter is large in the CxSM, and a large δ_2 , which is the mixing parameter between the SM Higgs and the singlet scalar S , is favored to realize strong first-order EWPT. On the other hand, a small δ_2 achieved through the degenerate scalar scenario suppresses the DM-quark scattering, so these two give contradictory conditions for the parameters. To explain them simultaneously, the DM mass needs to be half the Higgs mass, but here, the DM relic abundance is very small due to the resonance effect of the DM annihilation process and is far from the observed value $\Omega_{\text{DM}}h^2 = 0.1200 \pm 0.0012$ [20].

In this paper, we consider a model in which an $SU(2)_L$ doublet scalar and a complex singlet scalar are added to the SM. Since this model is the two-Higgs doublet model (2HDM) with the complex singlet S , we refer to this model as 2HDMS. In the 2HDMS, the CP-even scalars of the two Higgs doublet and the real part of S mix to form three Higgs particles $H_{1,2,3}$. The imaginary part of S acts as the DM. There are studies on 2HDMS, such as [21–24], but in these models, S has the Z_2 symmetry and may suffer from the domain wall problem, so here we introduce a linear term for S that breaks the symmetry. Furthermore, since v_S becomes nonzero for any temperature due to $a_1 \neq 0$, the EWPT is also different from the model with $a_1 = 0$. As with the CxSM mentioned earlier, we investigate whether the DM-quark scattering is suppressed when the mediator’s masses are degenerate ($m_{H_1} \simeq m_{H_2} \simeq m_{H_3}$), in other words, we investigate the feasibility of the degenerate scalar scenario. We take into account four types of Yukawa interaction between the SM fermions and the $SU(2)_L$ doublet Higgs bosons, which are distinguished by the Z_2 charge of each fermion. In the 2HDMS, the one-loop effect is most important for strong first-order EWPT, unlike the CxSM, where the tree-level structure is extremely important. As a result, it is shown that the degenerate scalar scenario is sufficiently valid even in the parameter region where strong first-order EWPT is achieved. In order to resolve the conflict between the degenerate scalar scenario and strong first-order EWPT, a two-component DM model that adds a fermion DM to the CxSM is also being studied [25], but here we explain the current DM abundance using only

the pNG DM of the 2HDMS.

The structure of this paper is as follows. Sec. II gives a brief review of the 2HDMS. After introducing the degenerate scalar scenario in Sec. III, to discuss the compatibility of the degenerate scalar scenario and strong first-order EWPT, we qualitatively analyze EWPT in Sec. IV. Then, we numerically investigate the parameter region consistent from the perspective of DM and EWPT in Sec. V. Lastly, Sec. VI summarizes this study.

II. THE MODEL

In the 2HDMS, the scalar potential is given as

$$V_0 = V_{0,2\text{HDM}} + V_{0,S}. \quad (1)$$

The first term in r.h.s. in (1) contains only the doublet Higgs fields Φ_1 and Φ_2

$$\begin{aligned} V_{0,2\text{HDM}}(\Phi_1, \Phi_2) = & m_1^2 \Phi_1^\dagger \Phi_1 + m_2^2 \Phi_2^\dagger \Phi_2 - \left(m_3^2 \Phi_1^\dagger \Phi_2 + \text{h.c.} \right) \\ & + \frac{\lambda_1}{2} \left(\Phi_1^\dagger \Phi_1 \right)^2 + \frac{\lambda_2}{2} \left(\Phi_2^\dagger \Phi_2 \right)^2 + \lambda_3 \left(\Phi_1^\dagger \Phi_1 \right) \left(\Phi_2^\dagger \Phi_2 \right) \\ & + \lambda_4 \left(\Phi_1^\dagger \Phi_2 \right) \left(\Phi_2^\dagger \Phi_1 \right) + \left[\frac{\lambda_5}{2} \left(\Phi_1^\dagger \Phi_2 \right)^2 + \text{h.c.} \right], \end{aligned} \quad (2)$$

where only m_3^2 term breaks the Z_2 symmetry of the doublets ($\Phi_1 \rightarrow +\Phi_1$, $\Phi_2 \rightarrow -\Phi_2$) softly.

The second term in (1) is given by the singlet S and doublets as

$$\begin{aligned} V_{0,S}(\Phi_1, \Phi_2, S) = & \frac{\delta_1}{2} \Phi_1^\dagger \Phi_1 |S|^2 + \frac{\delta_2}{2} \Phi_2^\dagger \Phi_2 |S|^2 + \frac{b_2}{2} |S|^2 + \frac{d_2}{4} |S|^4 \\ & + \left(a_1 S + \frac{b_1}{4} S^2 + \text{h.c.} \right), \end{aligned} \quad (3)$$

where the terms in the first line are invariant under a global U(1) transformation ($S \rightarrow e^{i\theta} S$), and terms in the second line break the symmetry softly. In the following, the scalar potential is assumed to be CP-invariant, i.e., all coefficients are real. Three scalar fields Φ_i ($i = 1, 2$) and S can be written as

$$\Phi_i = \left(\begin{array}{c} \phi_i^+ \\ \frac{1}{\sqrt{2}}(v_i + h_i + i\eta_i) \end{array} \right), \quad S = \frac{1}{\sqrt{2}}(v_S + s + i\chi). \quad (4)$$

At this time, $v = \sqrt{v_1^2 + v_2^2} = 246.22$ GeV and $\tan \beta = v_2/v_1$ is defined. The following scalar particles are present in this model; the charged scalar (ϕ_i^+), the CP-odd scalar (η_i),

and the CP-even scalars (h_1, h_2, s) . On the other hand, a pseudoscalar χ is the physical DM candidate.

First derivatives of V_0 with respect to h_1, h_2 and s are respectively given by

$$\left\langle \frac{\partial V_0}{\partial h_1} \right\rangle = m_1^2 v_1 - m_3^2 v_2 + \frac{\lambda_1}{2} v_1^3 + \frac{\lambda_{345}}{2} v_1 v_2^2 + \frac{\delta_1}{4} v_1 v_S^2 = 0, \quad (5)$$

$$\left\langle \frac{\partial V_0}{\partial h_2} \right\rangle = m_2^2 v_2 - m_3^2 v_1 + \frac{\lambda_2}{2} v_2^3 + \frac{\lambda_{345}}{2} v_1^2 v_2 + \frac{\delta_2}{4} v_2 v_S^2 = 0, \quad (6)$$

$$\left\langle \frac{\partial V_0}{\partial s} \right\rangle = \sqrt{2} a_1 + \frac{b_1 + b_2}{2} v_S + \frac{\delta_1}{4} v_1^2 v_S + \frac{\delta_2}{4} v_2^2 v_S + \frac{d_2}{4} v_S^3 = 0, \quad (7)$$

where $\lambda_{345} = \lambda_3 + \lambda_4 + \lambda_5$. The tree-level masses of the CP-even scalars are obtained by

$$\begin{aligned} -\mathcal{L}_{\text{mass}} &= \frac{1}{2} \begin{pmatrix} h_1 & h_2 & s \end{pmatrix} \mathcal{M}_S^2 \begin{pmatrix} h_1 \\ h_2 \\ s \end{pmatrix} = \frac{1}{2} \begin{pmatrix} H_1 & H_2 & H_3 \end{pmatrix} O^\top \mathcal{M}_S^2 O \begin{pmatrix} H_1 \\ H_2 \\ H_3 \end{pmatrix} \\ &= \frac{1}{2} \sum_{i=1}^3 m_{H_i}^2 H_i^2, \end{aligned} \quad (8)$$

with

$$\mathcal{M}_S^2 = \begin{pmatrix} m_3^2 \frac{v_2}{v_1} + \lambda_1 v_1^2 & -m_3^2 + \lambda_{345} v_1 v_2 & \frac{\delta_1}{2} v_1 v_S \\ -m_3^2 + \lambda_{345} v_1 v_2 & m_3^2 \frac{v_1}{v_2} + \lambda_2 v_2^2 & \frac{\delta_2}{2} v_2 v_S \\ \frac{\delta_1}{2} v_1 v_S & \frac{\delta_2}{2} v_2 v_S & -\frac{\sqrt{2} a_1}{v_S} + \frac{d_2}{2} v_S^2 \end{pmatrix}, \quad (9)$$

The mixing matrix O is parametrized as

$$O(\alpha_i) = \begin{pmatrix} 1 & 0 & 0 \\ 0 & c_3 & -s_3 \\ 0 & s_3 & c_3 \end{pmatrix} \begin{pmatrix} c_2 & 0 & -s_2 \\ 0 & 1 & 0 \\ s_2 & 0 & c_2 \end{pmatrix} \begin{pmatrix} c_1 & -s_1 & 0 \\ s_1 & c_1 & 0 \\ 0 & 0 & 1 \end{pmatrix}, \quad (10)$$

where $s_i = \sin \alpha_i$ and $c_i = \cos \alpha_i$ ($i = 1, 2, 3$). Note that the mixing matrix is orthogonal, i.e.,

$$\sum_k O_{ik} O_{jk} = \delta_{ij}. \quad (11)$$

Three Higgs particles appear in the 2HDMS, and H_1 is the Higgs boson observed at the LHC experiment.

On the other hand, the charged Higgs H^\pm and the CP-odd scalar A are defined from $\phi_{1,2}^+$, $\eta_{1,2}$ as

$$\begin{pmatrix} \phi_1^+ \\ \phi_2^+ \end{pmatrix} = R(\beta) \begin{pmatrix} G^+ \\ H^+ \end{pmatrix}, \quad \begin{pmatrix} \eta_1 \\ \eta_2 \end{pmatrix} = R(\beta) \begin{pmatrix} G^0 \\ A \end{pmatrix}, \quad (12)$$

where

$$R(\beta) = \begin{pmatrix} \cos \beta & -\sin \beta \\ \sin \beta & \cos \beta \end{pmatrix}. \quad (13)$$

In (12), G^\pm and G^0 denote Nambu-Goldstone bosons. The mass eigenvalues of H^\pm and A are given by

$$m_{H^\pm}^2 = \frac{m_3^2}{\sin \beta \cos \beta} - \frac{1}{2} (\lambda_4 + \lambda_5) v^2, \quad (14)$$

$$m_A^2 = \frac{m_3^2}{\sin \beta \cos \beta} - \lambda_5 v^2, \quad (15)$$

respectively. Also, DM mass is given by

$$m_\chi^2 = -\frac{\sqrt{2}a_1}{v_S} - b_1. \quad (16)$$

Let us summarize our input parameters. There are 14 degrees of freedom in the scalar potential: $\{m_1^2, m_2^2, m_3^2, \lambda_1, \lambda_2, \lambda_3, \lambda_4, \lambda_5, \delta_1, \delta_2, b_2, d_2, a_1, b_1\}$. First, $\{m_3^2, a_1\}$ remain as input parameters. $\{m_1^2, m_2^2, b_2\}$ are determined by the tadpole conditions (5)-(7) and $\{\lambda_4, \lambda_5, b_1\}$ are fixed by the particle masses (14),(15) and (16). The other six Lagrangian parameters are determined by the mass matrix of the CP-even scalars. In Appendix A, we list relationships between the input parameters and original Lagrangian parameters.

In order to prevent the tree-level FCNC in this model, we consider the case where one of the doublets couples with each fermion [26]. The Lagrangian of the Yukawa interaction is given as follows:

$$-\mathcal{L}_{\text{Yukawa}} = \bar{Q}_L Y_u \tilde{\Phi}_u u_R + \bar{Q}_L Y_d \Phi_d d_R + \bar{L}_L Y_\ell \Phi_\ell \ell_R + \text{h.c.}, \quad (17)$$

where $\Phi_f (f = u, d, \ell)$ is a Higgs doublet that couples to the fermion f and $\tilde{\Phi}_u \equiv i\sigma_2 \Phi_u^*$ and σ_2 being the Pauli matrix. Q_L and L_L represent left-handed quarks and left-handed leptons, i.e., $Q_L = (u_L, d_L)^\top$, $L_L = (\nu_L, e_L)^\top$. u_R , d_R , and ℓ_R are right-handed up-type quarks, right-handed down-type quarks, and right-handed leptons. $Y_f (f = u, d, \ell)$ is the 3×3 Yukawa matrix of the fermions. As shown in Table I, by assigning the Z_2 charge for the fermions, we can determine the combination of $\Phi_f (f = u, d, \ell)$ and classify them into four types.

	Q_L, L_L	u_R	d_R	ℓ_R	Φ_u	Φ_d	Φ_l
Type-I	+	-	-	-	Φ_2	Φ_2	Φ_2
Type-II	+	-	+	+	Φ_2	Φ_1	Φ_1
Type-X	+	-	-	+	Φ_2	Φ_2	Φ_1
Type-Y	+	-	+	-	Φ_2	Φ_1	Φ_2

TABLE I. Assignment of Z_2 charge to the fermions and combination of the doublets that couples to each fermion. The Higgs doublets Φ_1 and Φ_2 transform as $\Phi_1 \rightarrow +\Phi_1$ and $\Phi_2 \rightarrow -\Phi_2$, respectively.

III. DEGENERATE SCALAR SCENARIO

We study a suppression mechanism of the scattering process of DM χ off a quark q

$$\chi(p_1) + q(p_2) \rightarrow \chi(p_3) + q(p_4) \quad (18)$$

in the 2HDMS. The scattering amplitude \mathcal{M} is given by a sum of three amplitudes $\mathcal{M}_1, \mathcal{M}_2$ and \mathcal{M}_3 mediated by H_1, H_2 and H_3 , respectively:

$$i\mathcal{M} = i(\mathcal{M}_1 + \mathcal{M}_2 + \mathcal{M}_3), \quad (19)$$

$$i\mathcal{M}_1 = -i2C_{\chi\chi H_1}C_{qqH_1}\frac{1}{t - m_{H_1}^2}\bar{u}(p_4)u(p_2), \quad (20)$$

$$i\mathcal{M}_2 = -i2C_{\chi\chi H_2}C_{qqH_2}\frac{1}{t - m_{H_2}^2}\bar{u}(p_4)u(p_2), \quad (21)$$

$$i\mathcal{M}_3 = -i2C_{\chi\chi H_3}C_{qqH_3}\frac{1}{t - m_{H_3}^2}\bar{u}(p_4)u(p_2). \quad (22)$$

Here, $C_{S_1S_2S_3}$ denotes the scalar trilinear coupling for S_1, S_2 and S_3 , i.e., $\mathcal{L} \supset C_{S_1S_2S_3}S_1S_2S_3$. Thus, $C_{\chi\chi H_i}$ is the three-point scalar coupling between two χ and H_i ($i = 1, 2, 3$). On the other hand, C_{qqH_i} is the Yukawa coupling between the SM quarks q and H_i , $\mathcal{L} \supset C_{qqH_i}\bar{q}_Lq_RH_i$. A variable t describes a momentum transfer, $t \equiv (p_1 - p_3)^2$, and $u(p)$ ($\bar{u}(p)$) represents an incoming (outgoing) quark spinor with a momentum p . A factor 2 in the right-hand side of (20), (21) and (22) is a symmetry factor for the $\chi\chi H_i$ vertex.

First, we evaluate the degenerate scalar scenario in the mass eigenstates, and then use the gauge eigenstate to understand this scenario better. In the 2HDMS, the scalar trilinear couplings are given as follows:

$$C_{\chi\chi H_i} = \frac{1}{2v_S} \left(m_{H_i}^2 + \frac{\sqrt{2}a_1}{v_S} \right) O_{3i}, \quad (23)$$

which is derived from Eq. (8). On the other hand, the Yukawa interactions can be expressed as

$$C_{qqH_i} = \begin{cases} \frac{m_q}{v_1} O_{1i} & \text{(When } q \text{ couples to } \Phi_1), \\ \frac{m_q}{v_2} O_{2i} & \text{(When } q \text{ couples to } \Phi_2), \end{cases} \quad (24)$$

where m_q is the mass of quark q . Therefore, the amplitude (19) becomes

$$i\mathcal{M} = \begin{cases} -i2\frac{1}{2v_S} \sum_{i=1}^3 \frac{m_{H_i}^2 + \frac{\sqrt{2}a_1}{v_S}}{t - m_{H_i}^2} O_{3i} O_{1i} \bar{u}(p_4) u(p_2) & \text{(When } q \text{ couples to } \Phi_1), \\ -i2\frac{1}{2v_S} \sum_{i=1}^3 \frac{m_{H_i}^2 + \frac{\sqrt{2}a_1}{v_S}}{t - m_{H_i}^2} O_{3i} O_{2i} \bar{u}(p_4) u(p_2) & \text{(When } q \text{ couples to } \Phi_2). \end{cases} \quad (25)$$

If $a_1 = 0$, the amplitude vanishes in the low-energy limit ($t \rightarrow 0$) due to the orthogonality of the mixing matrix (11). However, as mentioned above, in order to avoid the domain wall problem associated with the development of v_S , we are currently setting a_1 to a nonzero value. In this case, the Higgs masses m_{H_i} must be degenerate to suppress the amplitude. This is the mechanism we call the degenerate scalar scenario.

Next, we discuss the degenerate scalar scenario in the gauge eigenstates to explore the origin of this mechanism. The doublets that couple to each fermion differ depending on the types in the 2HDMS. Therefore, we investigate the suppression mechanism for (A) and (B):

- (A) Type-I, Type-X : both up- and down-type quarks couple to Φ_2
- (B) Type-II, Type-Y : up (down)-type quark couples to Φ_2 (Φ_1)

A. Type-I, Type-X

The Yukawa interaction for Type-I and Type-X is given by

$$-\mathcal{L}_{\text{Yukawa}} = \sum_{i=1}^3 C_{uuH_i} \bar{u}_L u_R H_i + \sum_{i=1}^3 C_{ddH_i} \bar{d}_L d_R H_i + \text{h.c.}, \quad (26)$$

where

$$C_{uuH_i} = \frac{m_u}{v_2} O_{2i}, \quad C_{ddH_i} = \frac{m_d}{v_2} O_{2i}, \quad (27)$$

with $m_{u,d}$ being masses of up-type and down-type quarks. Here, the lepton sector is omitted since we focus only on the scattering with quarks. On the other hand, the scalar trilinear

interaction between χ and H_i is described by

$$\begin{aligned} -\mathcal{L} &\supset C_{\chi\chi h_1} h_1 \chi^2 + C_{\chi\chi h_2} h_2 \chi^2 + C_{\chi\chi s} s \chi^2 \\ &= C_{\chi\chi H_i} H_i \chi^2, \end{aligned} \quad (28)$$

where

$$C_{\chi\chi H_i} \equiv C_{\chi\chi h_1} O_{1i} + C_{\chi\chi h_2} O_{2i} + C_{\chi\chi s} O_{3i}. \quad (29)$$

Explicit expression of these couplings are summarized in Appendix B. Since the momentum transfer t in the direct detection experiments is very small as compared to the mediator masses, i.e., $t \ll m_{H_i}^2$, the amplitudes related to up-type quarks and down-type quarks can each be written by

$$\begin{aligned} i\mathcal{M}_{\text{up}} &= 2i\bar{u}(p_4) u(p_2) \frac{m_u}{v_2} \sum_{i=1}^3 \frac{C_{\chi\chi H_i} O_{2i}}{m_{H_i}^2}, \\ &= 2i\bar{u}(p_4) u(p_2) \frac{m_u}{v_2} \sum_{i=1}^3 \left(C_{\chi\chi h_1} \frac{O_{1i} O_{2i}}{m_{H_i}^2} + C_{\chi\chi h_2} \frac{O_{2i}^2}{m_{H_i}^2} + C_{\chi\chi s} \frac{O_{3i} O_{2i}}{m_{H_i}^2} \right), \end{aligned} \quad (30)$$

$$\begin{aligned} i\mathcal{M}_{\text{down}} &= 2i\bar{u}(p_4) u(p_2) \frac{m_d}{v_2} \sum_{i=1}^3 \frac{C_{\chi\chi H_i} O_{2i}}{m_{H_i}^2}, \\ &= 2i\bar{u}(p_4) u(p_2) \frac{m_d}{v_2} \sum_{i=1}^3 \left(C_{\chi\chi h_1} \frac{O_{1i} O_{2i}}{m_{H_i}^2} + C_{\chi\chi h_2} \frac{O_{2i}^2}{m_{H_i}^2} + C_{\chi\chi s} \frac{O_{3i} O_{2i}}{m_{H_i}^2} \right). \end{aligned} \quad (31)$$

Therefore, when three Higgs masses are degenerate, due to the orthogonality of the mixing matrix (11), the terms that are proportional to $O_{1i} O_{2i}$ and $O_{3i} O_{2i}$ vanish. On the other hand, the term that is proportional to O_{2i}^2 includes $C_{\chi\chi h_2}$. In this model, $C_{\chi\chi h_2}$ can be expressed as

$$C_{\chi\chi h_2} = \frac{\delta_2}{4} v_2, \quad (32)$$

where

$$\delta_2 = \frac{2}{v_2 v_S} \sum_{i=1}^3 O_{2i} O_{3i} m_{H_i}^2. \quad (33)$$

δ_2 is also suppressed by the orthogonality of the mixing matrix. Therefore, the amplitudes vanish in the degenerate scalar scenario ($m_{H_1} = m_{H_2} = m_{H_3}$). However, note that this suppression mechanism may not work well when v_2 and v_S , which appear in the denominator of Eq. (33), are very small.

We comment on the sum rule for the degenerate scalar scenario. The scattering of DM and quarks for case A (Type-I, Type-X) is as shown in Fig. 1. The left side uses the mass eigenstates, while the right side uses the gauge eigenstates. In order for the scalar h_1 and

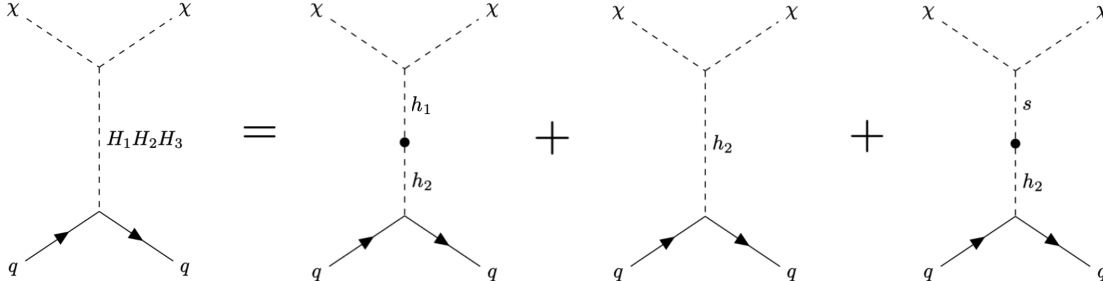


FIG. 1. Feynman diagrams of the DM-quark scattering in the mass and gauge eigenstates of scalar mediators. Both up-type quarks and down-type quarks couple to Φ_2 in case A (Type-I, Type-X).

s to couple with the quarks q , h_1 and s must be converted into h_2 through the couplings $C_{h_1h_2}$ and C_{h_2s} (the left and right diagram of the right-handed side in Fig. 1). On the other hand, the amplitude mediated by h_2 is proportional to the coupling $C_{\chi\chi h_2}$ (the middle of the right-handed side diagram in Fig. 1).

The scalar potential in the 2HDMS allows us to rewrite the trilinear couplings $C_{\chi\chi h_1}$, $C_{\chi\chi h_2}$ and $C_{\chi\chi s}$ by the bilinear couplings C_{h_1s} , C_{h_2s} and C_{ss} as

$$C_{\chi\chi h_1} = \frac{A}{v_S} (C_{h_1s} + \Delta_1), \quad C_{\chi\chi h_2} = \frac{A}{v_S} (C_{h_2s} + \Delta_2), \quad C_{\chi\chi s} = \frac{A}{v_S} (C_{ss} + \Delta_3), \quad (34)$$

where parameters A , Δ_1 , Δ_2 and Δ_3 are expressed by parameters besides C_{h_1s} , C_{h_2s} and C_{ss} in the scalar potential. The bilinear couplings are also given in Appendix B. Referring to Eqs. (30), (31) and extracting the part that is involved in suppressing the scattering, one gets

$$\begin{aligned} \frac{C_{\chi\chi H_i} O_{2i}}{m_{H_i}^2} &= \frac{A}{v_S} \{ (C_{h_1s} + \Delta_1) O_{1i} + (C_{h_2s} + \Delta_2) O_{2i} + (C_{ss} + \Delta_3) O_{3i} \} \frac{O_{2i}}{m_{H_i}^2}, \\ &= \frac{A}{v_S m_{H_i}^2} (O_{3i} O_{2i} m_{H_i}^2 + \Delta_1 O_{1i} O_{2i} + \Delta_2 O_{2i}^2 + \Delta_3 O_{3i} O_{2i}), \end{aligned} \quad (35)$$

where we use relations of coefficients between the gauge and mass eigenstates, i.e., $C_{h_1s} O_{1i} + C_{h_2s} O_{2i} + C_{ss} O_{3i} = O_{3i} m_{H_i}^2$.¹ Therefore, the amplitude in the degenerate Higgs region

¹ This formula is derived from $O^\top M_S^2 O = \sum_{i=1}^3 m_{H_i}^2$ related to Eq. (8).

vanishes when

$$\Delta_2 = 0. \quad (36)$$

We show that the condition (36) holds for the scalar potential V_0 (1). In the 2HDMS, the couplings C_{h_2s} and $C_{\chi\chi h_2}$ are related to

$$\begin{aligned} V_0 &\supset \frac{\delta_2}{2} \Phi_2^\dagger \Phi_2 |S|^2 \\ &\supset C_{\chi\chi h_2} h_2 \chi^2 + C_{h_2s} h_2 s, \end{aligned} \quad (37)$$

where

$$C_{\chi\chi h_2} = \frac{\delta_2}{4} v_2, \quad C_{h_2s} = \frac{\delta_2}{2} v_2 v_S. \quad (38)$$

Comparing (38) with (34), we find

$$A = \frac{1}{2}, \quad \Delta_2 = 0. \quad (39)$$

Therefore, in the degenerate limit of the mediator masses, the DM-quark scattering is suppressed as long as the potential (1) is used. In other words, the mixing term between Φ_2 and S is constrained by the degenerate scalar scenario. For example, suppose that the mixing terms $\frac{c_2}{4} \Phi_2^\dagger \Phi_2 S$ is added to the potential (1). The couplings $C_{\chi\chi h_2}$ and C_{h_2s} become

$$C_{\chi\chi h_2} = \frac{\delta_2}{4} v_2, \quad C_{h_2s} = \frac{\delta_2}{2} v_2 v_S + \frac{\sqrt{2} c_2}{4} v_2. \quad (40)$$

Then,

$$A = \frac{1}{2}, \quad \Delta_2 = -\frac{\sqrt{2} c_2}{4} v_2, \quad (41)$$

which is inconsistent with the condition (36). Thus, if the mixing terms such as $\Phi_2^\dagger \Phi_2 S$, $\Phi_2^\dagger \Phi_2 S^2$ are added, the suppression mechanism does not work.²

B. Type-II, Type-Y

The Yukawa interaction for Type-II and Type-Y is given by

$$-\mathcal{L}_{\text{Yukawa}} = \sum_{i=1}^3 C_{uuH_i} \bar{u}_L u_R H_i + \sum_{i=1}^3 C_{ddH_i} \bar{d}_L d_R H_i + \text{h.c.}, \quad (42)$$

² A more detailed analysis, including one-loop scattering, is given in Ref. [27]. This discussion can be applied almost directly to the case of the 2HDMS.

where

$$C_{uuH_i} = \frac{m_u}{v_2} O_{2i}, \quad C_{ddH_i} = \frac{m_d}{v_1} O_{1i}. \quad (43)$$

The amplitude becomes

$$\begin{aligned} i\mathcal{M}_{\text{up}} &= 2i\bar{u}(p_4) u(p_2) \frac{m_u}{v_2} \sum_{i=1}^3 \frac{C_{\chi\chi H_i} O_{2i}}{m_{H_i}^2} \\ &= 2i\bar{u}(p_4) u(p_2) \frac{m_u}{v_2} \sum_{i=1}^3 \left(C_{\chi\chi h_1} \frac{O_{1i} O_{2i}}{m_{H_i}^2} + C_{\chi\chi h_2} \frac{O_{2i}^2}{m_{H_i}^2} + C_{\chi\chi s} \frac{O_{3i} O_{2i}}{m_{H_i}^2} \right), \end{aligned} \quad (44)$$

$$\begin{aligned} i\mathcal{M}_{\text{down}} &= 2i\bar{u}(p_4) u(p_2) \frac{m_d}{v_1} \sum_{i=1}^3 \frac{C_{\chi\chi H_i} O_{1i}}{m_{H_i}^2} \\ &= 2i\bar{u}(p_4) u(p_2) \frac{m_d}{v_1} \sum_{i=1}^3 \left(C_{\chi\chi h_1} \frac{O_{1i}^2}{m_{H_i}^2} + C_{\chi\chi h_2} \frac{O_{2i} O_{1i}}{m_{H_i}^2} + C_{\chi\chi s} \frac{O_{3i} O_{1i}}{m_{H_i}^2} \right). \end{aligned} \quad (45)$$

As for case A (Type-I, Type-X), this scattering is suppressed when the three Higgs masses are equal. In order to suppress the down-type quarks scattering, it is necessary to suppress $C_{\chi\chi h_1}$, which can be expressed as

$$C_{\chi\chi h_1} = \frac{\delta_1}{4} v_1, \quad (46)$$

with

$$\delta_1 = \frac{2}{v_1 v_S} \sum_{i=1}^3 O_{1i} O_{3i} m_{H_i}^2. \quad (47)$$

Thus, in the degenerate scalar scenario, it is important to suppress δ_2 for the up-type scattering and δ_1 for the down-type scattering.

We also mention the sum rule for the degenerate scalar scenario in this case. The scattering of DM and quarks for case B (Type-II, Type-Y) is as shown in Fig. 2 and up-type quarks u and down-type quarks d couple to the different Higgs doublet. The scattering of up-type quarks is the same as the discussion of case A, so we focus on those of down-type quarks. As can be seen from Eq. (45), the relevant part of the suppression mechanism is

$$\begin{aligned} \frac{C_{\chi\chi H_i} O_{1i}}{m_{H_i}^2} &= \frac{A}{v_S} \{ (C_{h_1 s} + \Delta_1) O_{1i} + (C_{h_2 s} + \Delta_2) O_{2i} + (C_{s s} + \Delta_3) O_{3i} \} \frac{O_{1i}}{m_{H_i}^2}, \\ &= \frac{A}{v_S m_{H_i}^2} (O_{3i} O_{1i} m_{H_i}^2 + \Delta_1 O_{1i}^2 + \Delta_2 O_{2i} O_{1i} + \Delta_3 O_{3i} O_{1i}). \end{aligned} \quad (48)$$

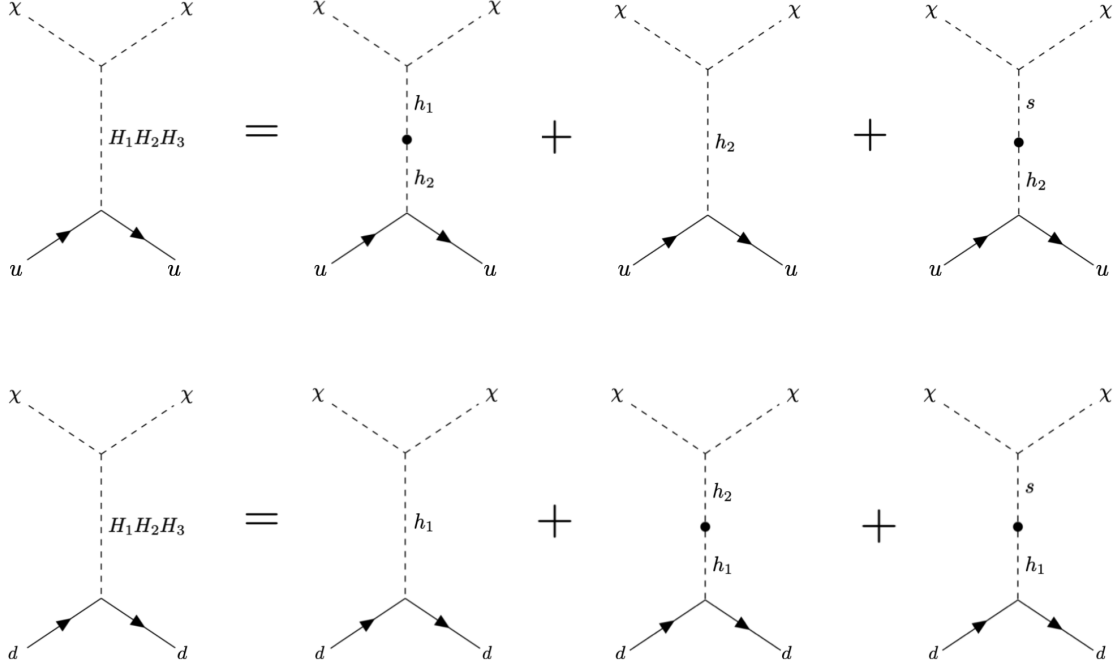


FIG. 2. Feynman diagrams of the DM-quark scattering in the mass and gauge eigenstates of scalar mediators. Up-type quarks u couple to Φ_2 , while down-type quarks d couple to Φ_1 in case B (Type-II, Type-Y).

In this case, the amplitude in the degenerate Higgs region vanishes when

$$\Delta_1 = 0 \quad (49)$$

In the 2HDMS, the couplings $C_{h_1 s}$ and $C_{\chi\chi h_1}$ are related to

$$\begin{aligned} V_0 &\supset \frac{\delta_1}{2} \Phi_1^\dagger \Phi_1 |S|^2 \\ &\supset C_{\chi\chi h_1} h_1 \chi^2 + C_{h_1 s} h_1 s, \end{aligned} \quad (50)$$

where

$$C_{\chi\chi h_1} = \frac{\delta_1}{4} v_1, \quad C_{h_1 s} = \frac{\delta_1}{2} v_1 v_S. \quad (51)$$

Comparing (51) with (34), we find

$$A = \frac{1}{2}, \quad \Delta_1 = 0. \quad (52)$$

Thus, in the degenerate scalar scenario, the DM-quark scattering is suppressed with the potential (1) same as case A.

C. Higgs search

We mention the usefulness of the degenerate scalar scenario in the Higgs search experiments at the LHC. In the 2HDMS, the couplings between the Higgs boson H_i and the SM particle X are given by the SM couplings multiplied by the mixing matrix elements O_{1i} . Taking the decay widths of H_i as an example, we obtain

$$\Gamma_{H_1 \rightarrow XX} = \Gamma_{h \rightarrow XX}^{\text{SM}}(m_{H_1}) \times O_{11}^2, \quad (53)$$

$$\Gamma_{H_2 \rightarrow XX} = \Gamma_{h \rightarrow XX}^{\text{SM}}(m_{H_2}) \times O_{12}^2, \quad (54)$$

$$\Gamma_{H_3 \rightarrow XX} = \Gamma_{h \rightarrow XX}^{\text{SM}}(m_{H_3}) \times O_{13}^2, \quad (55)$$

where $\Gamma_{h \rightarrow XX}^{\text{SM}}(m_{H_i})$ is the decay width of the SM Higgs h as a function of m_{H_i} . When we add up all the decay widths with $m_{H_i} \simeq m_h = 125$ GeV,

$$\Gamma_{H_1 \rightarrow XX} + \Gamma_{H_2 \rightarrow XX} + \Gamma_{H_3 \rightarrow XX} \simeq \Gamma_{h \rightarrow XX}^{\text{SM}}(m_h) \quad (56)$$

is obtained. This SM-like process is effective for all mixing angles, and H_i cannot be distinguished in the current experiment [4].

IV. QUALITATIVE DISCUSSION FOR ELECTROWEAK PHASE TRANSITION

We discuss the compatibility of the degenerate scalar scenario and EWPT qualitatively. As mentioned in Sec. III, the orthogonality of the mixing matrix (11) is important for the degenerate scalar scenario. Here, using the elements of the mixing matrix, the mixing parameters for $\text{SU}(2)_L$ doublet-singlet in the scalar potential can be expressed as

$$\delta_1 = \frac{2}{v_1 v_S} (O_{1i} O_{3i} m_{H_i}^2), \quad (57)$$

$$\delta_2 = \frac{2}{v_2 v_S} (O_{2i} O_{3i} m_{H_i}^2). \quad (58)$$

As we discussed in Sec. III, it can be seen that the DM-quark scattering is controlled by δ_1 and δ_2 . In other words, the degenerate scalar scenario is realized by δ_1 and δ_2 . Strong first-order EWPT is essential for EWBG, and the condition is [28–30];

$$\frac{v_C}{T_C} \gtrsim 1, \quad (59)$$

where T_C is the critical temperature at which the effective potential has two degenerate minima, and $v_C = \sqrt{v_{1C}^2 + v_{2C}^2}$ is the nonzero Higgs VEV at $T = T_C$. Possible origins of first-order EWPT are the finite-temperature boson loop and the structure of the tree-level potential. In the former case, the addition of multiple bosons is effective, and the 2HDM specializes in this type of EWPT. On the other hand, in the latter case, the existence of a single scalar is important, and the CxSM causes this type of EWPT. Since the 2HDMS has multiple bosons and a singlet scalar that does not exist in the SM, EWPT of both types can occur. First, we qualitatively analyze tree-level driven EWPT using the so-called high temperature (HT) potential, which is composed of the tree-level potential and thermal masses. In the high-temperature expansion of the finite temperature effective potential, we can obtain not only the thermal masses but also the thermal cubic terms. However, here, we only add the thermal masses to the tree-level potential since we want to check whether first-order EWPT occurs due to the effect of the doublet-singlet mixing of the tree-level. Generally, first-order EWPT would be enhanced even more by adding the thermal cubic terms.

EWPT pattern of 2HDMS is $(\langle\Phi_1\rangle, \langle\Phi_2\rangle, \langle S\rangle) = (0, 0, v'_S) \rightarrow (v_1, v_2, v_S)$, where $\langle\Phi_i\rangle$ and $\langle S\rangle$ are defined as the VEVs of the doublet fields Φ_i and the singlet field S , respectively. To discuss EWPT, we take the Landau gauge and assume that the charged scalar bosons do not have VEVs at any temperature in order to conserve the $U(1)_{\text{QED}}$. We denote the classical background fields of the Higgs doublets and singlet as

$$\langle\Phi_i\rangle = \begin{pmatrix} 0 & \varphi_i \end{pmatrix}^\top / \sqrt{2}, \quad \langle S\rangle = \varphi_S / \sqrt{2}. \quad (60)$$

The tree-level potential (1) can be rewritten as

$$\begin{aligned} V_0(\varphi_1, \varphi_2, \varphi_S) &= \frac{m_1^2}{2}\varphi_1^2 + \frac{m_2^2}{2}\varphi_2^2 - m_3^2\varphi_1\varphi_2 + \frac{\lambda_1}{8}\varphi_1^4 + \frac{\lambda_2}{8}\varphi_2^4 + \frac{\lambda_{345}}{4}(\varphi_1\varphi_2)^2 \\ &+ \frac{\delta_1}{8}\varphi_1^2\varphi_S^2 + \frac{\delta_2}{8}\varphi_2^2\varphi_S^2 + \frac{b_2}{4}\varphi_S^2 + \frac{d_2}{16}\varphi_S^4 + \sqrt{2}a_1\varphi_S + \frac{b_1}{4}\varphi_S^2. \end{aligned} \quad (61)$$

The HT potential is defined as

$$V^{\text{HT}}(\varphi_1, \varphi_2, \varphi_S; T) = V_0(\varphi_1, \varphi_2, \varphi_S) + (\Sigma_{h1}\varphi_1^2 + \Sigma_{h2}\varphi_2^2 + \Sigma_S\varphi_S^2) T^2, \quad (62)$$

where

$$\Sigma_{h1} = \frac{\delta_1}{48} + \frac{g_1^2}{32} + \frac{3g_2^2}{32} + \frac{\lambda_1}{8} + \frac{\lambda_3}{12} + \frac{\lambda_4}{24} + \frac{y_t^2}{8} + \frac{y_b^2}{8}, \quad (63)$$

$$\Sigma_{h2} = \frac{\delta_2}{48} + \frac{g_1^2}{32} + \frac{3g_2^2}{32} + \frac{\lambda_2}{8} + \frac{\lambda_3}{12} + \frac{\lambda_4}{24} + \frac{y_t^2}{8} + \frac{y_b^2}{8}, \quad (64)$$

$$\Sigma_S = \frac{d_2}{24} + \frac{\delta_1}{24} + \frac{\delta_2}{24}, \quad (65)$$

with g_2, g_1, y_t and y_b being $SU(2)_L$, $U(1)_Y$, top Yukawa and bottom Yukawa couplings. It should be emphasized that the thermal cubic term of the field is necessary for loop-driven EWPT. Since the HT potential does not include that term, it is optimal for analyzing EWPT derived from the tree-level potential.

For convenience, φ_i and φ_S are parameterized as

$$\varphi_1 = z \cos \theta \cos \beta, \quad \varphi_2 = z \cos \theta \sin \beta, \quad \varphi_S = z \sin \theta + v'_S, \quad (66)$$

where v'_S denotes the minimum on the φ_S axis, which is always nonzero because of $a_1 \neq 0$ in our model. The HT potential (62) becomes

$$V^{\text{HT}}(z, \theta, \beta; T) = c_0 + c_1 z + (c_2 + c'_2 T^2) z^2 - c_3 z^3 + c_4 z^4. \quad (67)$$

Eq. (67) is composed of the tree-level potential and the thermal masses, and there is no thermal cubic term like $-c'_3 T z^3$. This means that strong first-order EWPT could be achieved even if $c'_3 = 0$ in this model. After shifting the vacuum energy with $c_0 = 0$, the above potential at $T = T_C$ takes the form

$$V^{\text{HT}}(z, \theta, \beta; T_C) = c_4 z^2 (z - z_C)^2, \quad z_C = \frac{c_3}{2c_4}, \quad (68)$$

where

$$c_3 = \frac{1}{4} v'_S \sin \theta (\delta_1 \cos^2 \beta \cos^2 \theta + \delta_2 \cos^2 \theta \sin^2 \beta + d_2 \sin^2 \theta), \quad (69)$$

$$c_4 = \frac{1}{16} (2\lambda_1 \cos^4 \beta \cos^4 \theta + 2\lambda_2 \cos^4 \theta \sin^4 \beta + 2\delta_2 \cos^2 \theta \sin^2 \beta \sin^2 \theta + d_2 \sin^4 \theta + 2 \cos^2 \beta (2\lambda_{345} \cos^4 \theta \sin^2 \beta + \delta_1 \cos^2 \theta \sin^2 \theta)). \quad (70)$$

From this potential, v_C and T_C are derived, which are

$$v_C = \sqrt{\frac{v'_{SC}(v'_{SC} - v_{SC})(\delta_1 \cos^2 \beta_C + \delta_2 \sin^2 \beta_C)}{\lambda_1 \cos^4 \beta_C + \lambda_2 \sin^4 \beta_C + 2\lambda_{345} \sin^2 \beta_C \cos^2 \beta_C}} \quad (71)$$

$$T_C = \sqrt{\frac{-m_1^2 \cos^2 \beta_C - m_2^2 \sin^2 \beta_C + 2m_3^2 \cos \beta_C \sin \beta_C - \frac{1}{4} v'_{SC} (\delta_1 \cos^2 \beta_C + \delta_2 \sin^2 \beta_C)}{\Sigma_{h1} \cos^2 \beta_C + \Sigma_{h2} \sin^2 \beta_C}}. \quad (72)$$

The physical quantities evaluated by T_C are labeled with the subscript C . We can find that the condition of strong first-order EWPT (59) requires large δ_1 and δ_2 . If, in Eq. (72), the following relation holds

$$-m_1^2 \cos^2 \beta_C - m_2^2 \sin^2 \beta_C + 2m_3^2 \cos \beta_C \sin \beta_C = 0, \quad (73)$$

it seems that v_C/T_C is independent from both δ_1 and δ_2 since the terms related to δ_1 and δ_2 are canceled out between v_C and T_C . However, there are δ_1 and δ_2 in Σ_{h1} (63) and Σ_{h2} (64), and large δ_1 and δ_2 are still preferred to satisfy the condition of strong first-order EWPT.

However, as mentioned above, small δ_1, δ_2 are essential for realizing the degenerate scalar scenario. Therefore, we do not entrust EWPT to the tree-level double-single mixing δ_1, δ_2 , but to the thermal loop. The 1-loop effective potential can be written as follows:

$$\begin{aligned} V_{\text{eff}}(\varphi_1, \varphi_2, \varphi_S; T) &= V_0(\varphi_1, \varphi_2, \varphi_S) + V_1(\varphi_1, \varphi_2, \varphi_S; T), \\ &= V_0(\varphi_1, \varphi_2, \varphi_S) + \sum_i n_i \left[V_{\text{CW}}(\bar{m}_i^2) + \frac{T^4}{2\pi^2} I_{B,F} \left(\frac{\bar{m}_i^2}{T^2} \right) \right], \end{aligned} \quad (74)$$

where T represents temperature. The subscript i represents the particles contained in the model, and n_i is the degree of freedom of each particle. The effective potentials at zero temperature and at the finite temperature are given by [31–33]

$$V_{\text{CW}}(\bar{m}_i^2) = \frac{\bar{m}_i^4}{64\pi^2} \left(\ln \frac{\bar{m}_i^2}{\bar{\mu}^2} - c_i \right), \quad (75)$$

$$I_{B,F}(a^2) = \int_0^\infty dx x^2 \ln \left(1 \mp e^{-\sqrt{x^2+a^2}} \right), \quad (76)$$

where $c_i = 3/2$ for scalars and fermions and $c_i = 5/6$ for gauge bosons. \bar{m}_i is the field-dependent masses of each particle i . I_B with the minus sign represents the boson contribution, while I_F with the plus sign represents the fermion one. $\bar{\mu}$ is a renormalization scale.

In the following calculations, the condition (59) is checked using the 1-loop effective potential (74). In order to prevent the breakdown of perturbation theory due to boson multi-loop, the Parwani resummation, in which all the Matsubara frequency modes are resummed, is used [34]. Specifically, field-dependent masses \bar{m}_i^2 in Eq. (74) are replaced by thermally corrected ones.

V. NUMERICAL RESULTS

Before giving benchmark points, we mention the theoretical and experimental constraints imposed on the parameters. A requirement on the scalar potential that is bounded from below is given by [35, 36]

$$\lambda_1 > 0, \lambda_2 > 0, \lambda_3 + \lambda_4 - \lambda_5 > -\sqrt{\lambda_1 \lambda_2}, d_2 > 0. \quad (77)$$

The quartic couplings should also satisfy the following conditions from the tree-level unitarity [37, 38]

$$\lambda_1 < \frac{8\pi}{3}, \lambda_2 < \frac{8\pi}{3}, \lambda_{345} < 8\pi, \delta_1 < 16\pi, \delta_2 < 16\pi, d_2 < \frac{16\pi}{3}. \quad (78)$$

The constraint from the perturbativity is as follows [39]:

$$|\lambda_j|, d_2 < 4\pi \quad (j = 1 - 5). \quad (79)$$

Furthermore, the sizes of δ_1 and δ_2 could be constrained by a global minimum condition at zero temperature [40]. The energy of the electroweak vacuum has to be lower than that of the local vacuum on the φ_S axis. Experimental constraints here are primarily related to electroweak precision data and flavor experiments. By assuming a mass degeneracy between the charged scalar boson H^\pm and the neutral scalar boson H or the CP-odd scalar boson A , i.e., $m_{H^\pm} \simeq m_H$ or m_A , the electroweak precision data is satisfied [41]. In addition, for Type-I 2HDMS, $B_d \rightarrow \mu\mu$ process requires $\tan\beta \gtrsim 1.75$ for $m_{H^\pm} = 500$ GeV [42]. We should emphasize that the Higgs coupling measurement usually places a constraint on $\cos(\beta - \alpha)$, but not now since our analysis is based on the degenerate scalar scenario.

The input and output parameters that satisfy the above constraints are summarized in Table II. The masses of three Higgs bosons are degenerate within 1 GeV. In addition, these three benchmark points (BPs) reflect the EWPT discussion in Sec. IV. The difference between input parameters among BPs is the size of v_S . The parameter a_1 is changed to keep the value of d_2 perturbatively appropriate. The observed DM relic density is known as [20]

$$\Omega_{\text{DM}} h^2 = 0.1200 \pm 0.0012, \quad (80)$$

and we choose the DM mass that reproduces this value at each BP.

The public code `cosmoTransitions` [43] is used to evaluate EWPT. In Table III, T_C and corresponding VEVs for BPs are shown, and strong first-order EWPT occurs in all BPs.

Inputs	v	v_S	m_{H_1}	m_{H_2}	m_{H_3}	m_{H^\pm}	m_A	m_χ	α_1	α_2	α_3	$\tan\beta$	a_1	m_3^2
BP1	246.22	246.22	125.0	124.5	124.0	500	500	140.19	$\pi/4$	$\pi/4$	0.01	2.0	-6550	10
BP2	246.22	200	125.0	124.5	124.0	500	500	130.85	$\pi/4$	$\pi/4$	0.01	2.0	-700000	10
BP3	246.22	30	125.0	124.5	124.0	500	500	122.60	$\pi/4$	$\pi/4$	0.01	2.0	-323000	10
Outputs	δ_1	δ_2	d_2	λ_1	λ_2	λ_3	λ_4	λ_5	m_1^2	m_2^2	b_1	b_2	v_1	v_2
BP1	0.0069	0.0017	0.51	1.27	0.32	8.25	-4.12	-4.12	-7863	-7812	-19616	4176	110	220
BP2	0.0085	0.0020	0.53	1.27	0.32	8.25	-4.12	-4.12	-7843	-7807	-12172	11450	110	220
BP3	0.057	0.014	0.54	1.27	0.32	8.25	-4.12	-4.12	-7771	-7790	195.6	29339	110	220

TABLE II. Input and output parameters. These BPs reproduce the observed DM relic density (80).

	v_{1C} [GeV]	v_{2C} [GeV]	v_{SC} [GeV]	v'_{SC} [GeV]	v_C/T_C
BP1	105.8	213.2	245.6	246.2	$\frac{238.0}{69.6} = 3.4$
BP2	105.8	213.2	199.5	200.1	$\frac{238.0}{69.6} = 3.4$
BP3	105.7	213.2	30.0	30.6	$\frac{238.0}{69.6} = 3.4$

TABLE III. T_C and corresponding VEVs for three BPs in Table II. Here, the calculations are performed by `cosmoTransitions` [43].

v_C/T_C is determined roughly by the ratio of the cubic and quartic terms of the field. The bosons masses are important for the former, and λ_i is important for the latter. Since the boson masses are almost the same and the value of λ_i is completely the same for all BPs, the Higgs VEVs and T_C are almost identical in three cases. In addition, the small change in the singlet VEV before and after EWPT shows that the tree-level effect by the singlet introduction does not cause EWPT this time. In fact, when using the HT potential (62), EWPT becomes second-order.

Next, we show the results of numerical calculations related to the DM using the public code `micrOMEGAs` [44, 45]. In Fig. 3, the spin-independent cross section for the scattering between the DM and nucleus σ_{SI} as a function of m_{H_2} is shown. Here, m_{H_2} is used once as a variable, and the other parameters are BPs in Table II. The shaded regions are excluded by the LZ experiment. For all BPs, there is a large dip around $m_{H_2} \simeq 125$ GeV. This indicates that the degenerate scalar scenario is important for the suppression of DM and

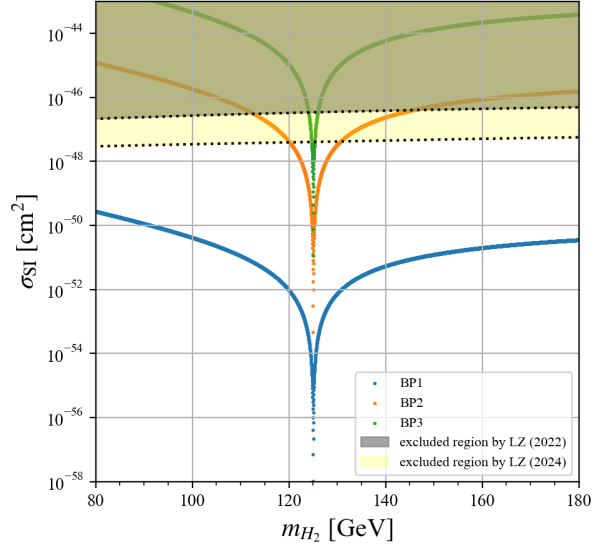


FIG. 3. Spin-independent cross section for the scattering between the DM and nucleus σ_{SI} as a function of m_{H_2} .

nucleon scattering. Although the value of δ_2 varies between the BPs, a_1 may be more closely controlling the overall magnitude of σ_{SI} . As can be seen from Eq. (25), σ_{SI} is proportional to a_1^2 . For example, the difference in σ_{SI} between BP1 and BP2 is roughly 10^4 , which is due to the fact that $a_1^2(\text{BP2})/a_1^2(\text{BP1}) \simeq 10^4$. a_1 is important for adjusting d_2 to an appropriate value, but it also affects the magnitude of σ_{SI} in this way. On the other hand, if the Higgs masses are degenerate, the scattering is suppressed regardless of the value of a_1 . In other words, the degenerate scalar scenario is also valid when $a_1 = 0$, but to avoid the domain wall problem, we should consider $a_1 \neq 0$. Thus, Although the elastic neutrino-nucleon scattering makes DM detection difficult in some regions, this does not rule out the existence of the WIMP-DM [46].

The left panel of Fig. 4 shows $\Omega_\chi h^2$ as a function of m_χ for all BPs in Table. II. The value of the DM relic density $\Omega_{\text{DM}} h^2$ must not exceed the observed value (80), corresponding to the black dashed line in the graph. The red dots indicate the points where the calculated value equals the observed value (80) and BPs are included.

On the other hand, the right panel of Fig. 4 shows the m_χ dependence of the spin-independent scattering cross section between DM and nucleus. For $\Omega_\chi < \Omega_{\text{DM}}$, we should

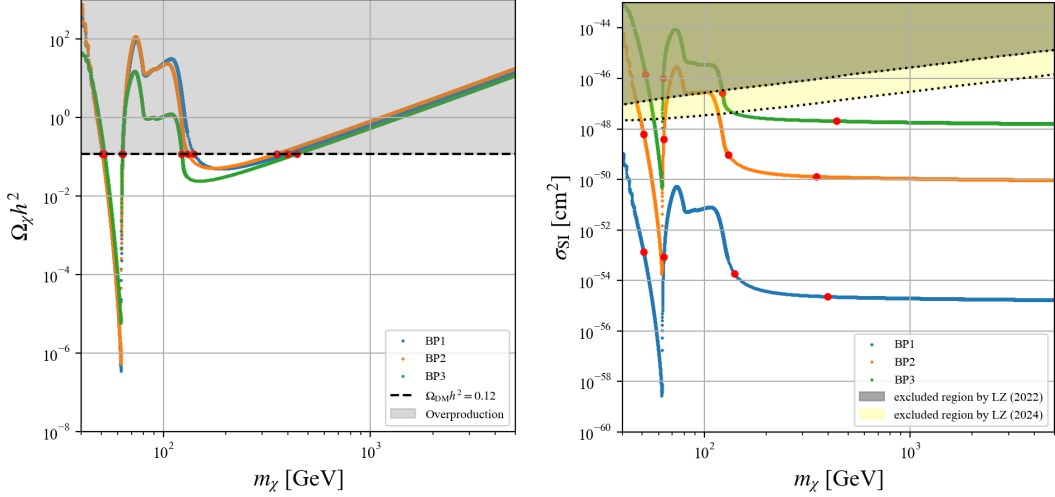


FIG. 4. (Left panel) DM relic density $\Omega_\chi h^2$ as a function of DM mass m_χ for the BPs in Table. II is shown. The black dashed line represents the observed value (80), and the region above this corresponds to overproduction. (Right panel) scaled scattering cross section between the DM χ and quarks $\tilde{\sigma}_{\text{SI}}$ as a function of DM mass m_χ for all BPs is shown. The dotted line represents the bound of the LZ experiment, and the region above this is excluded. The red dots on both panels indicate where the observed relic density and the predicted one from the 2HDMS are equal.

scale σ_{SI} as

$$\tilde{\sigma}_{\text{SI}} = \left(\frac{\Omega_\chi}{\Omega_{\text{DM}}} \right) \sigma_{\text{SI}}. \quad (81)$$

Here, the scaled cross section is shown for each BP. The dotted line is the bound of the LZ experiment, and the region above this is excluded. The red dots correspond to those of the left panel. It can be seen that many DM mass regions are still allowed, and the DM χ may carry all of the existing DM and explain the current experimental results.

VI. SUMMARY AND DISCUSSION

In this paper, we have investigated the compatibility of the degenerate scalar scenario and strong first-order EWPT in the 2HDMS, which contains two Higgs doublets and one singlet scalar. In this model, the imaginary part of S behaves as a DM χ , and CP-even scalars mix to form three Higgs particles H_i ($i = 1, 2, 3$). The scattering of DM and quarks is mediated by H_i , and we have found that this scattering is suppressed in the region where

	$\lambda_{111}/\lambda_{hhh}^{\text{SM}}$	$\lambda_{112}/\lambda_{hhh}^{\text{SM}}$	$\lambda_{113}/\lambda_{hhh}^{\text{SM}}$	$\Delta\lambda_{11}^{\text{total}}$
BP1	0.799	-0.00872	0.571	0.362
BP2	0.780	0.0109	0.544	0.335
BP3	0.701	0.0921	0.431	0.224

TABLE IV. The deviation from the SM values for the Higgs trilinear couplings λ_{111} , λ_{112} , λ_{113} and their sum defined as Eq. (83).

Higgs masses are degenerate, as shown in previous studies on pNG DM [4]. The suppression of $SU(2)_L$ doublet-singlet mixing terms δ_1 and δ_2 , which are related to the orthogonality of the mixing matrix that transforms the gauge eigenstates to the mass eigenstates of the CP-even scalars, is important for the degenerate scalar scenario.

Strong first-order EWPT, an essential element of EWBG, can be derived from two sources in the effective potential: the thermal loop and the tree-level structure. Since the tree-level driven EWPT is induced by the presence of the singlet field, i.e., large δ_1 , δ_2 are important, it was pointed out here that this is inconsistent with the degenerate scalar scenario (the discussion in the CxSM is given in ref. [19]). Therefore, as is common with the 2HDM, it is best to leave strong first-order EWPT to the loop effect.

We have set the benchmark points based on the qualitative discussion of EWPT and confirmed that strong first-order EWPT actually occurs. Since we focus on the degenerate scalar scenario, the DM-quark spin-independent cross section is suppressed even in regions that satisfy the DM observed relic density, and we were able to explain the constraint from the LZ experiment in many regions. Therefore, it was found that current observational data and experimental results can be explained by the DM χ in this model and that it is also consistent with the condition given by strong first-order EWPT.

Finally, we briefly discuss the possibility of verifying the model in future collider experiments. A distinctive feature of the thermal loop-derived EWPT is a shift of the Higgs trilinear coupling

$$\mathcal{L} = \lambda_{ijk} H_i H_j H_k \quad (i, j, k = 1, 2, 3), \quad (82)$$

from the SM prediction [47, 48]. For example, we focus on the pair production of H_1 through off-shell CP-even scalars H_i , i.e., $H_i \rightarrow H_1 H_1$. We compare each trilinear coupling λ_{11i} ($i = 1, 2, 3$) in three benchmark points (BP1, BP2, BP3) with the SM. Furthermore,

since amplitudes mediated by off-shell scalars H_i interfere with each other, we also compare the sum of trilinear couplings λ_{111} , λ_{112} and λ_{113} to the SM prediction. The results are shown in Table. IV, where $\Delta\lambda_{11}^{\text{total}}$ is defined as

$$\Delta\lambda_{11}^{\text{total}} = \frac{(\lambda_{111} + \lambda_{112} + \lambda_{113}) - \lambda_{hhh}^{\text{SM}}}{\lambda_{hhh}^{\text{SM}}}, \quad (83)$$

The Higgs trilinear coupling of this model is expected to differ from that of SM by about 30%, and it may be confirmed at the High-Energy Large Hadron Collider (HE-LHC) and/or the International Linear Collider (ILC), whose accuracy is estimated by ref. [49]. We leave the detailed analysis and the model verification in other experiments, such as the search for the degenerate Higgs at the lepton collider and observation of gravitational waves from EWPT, to future research.

ACKNOWLEDGMENTS

We are grateful to Ayana Okuma and Chiaki Nose for their valuable discussions. The work of GCC is supported by JSPS KAKENHI Grant No. 22K03616. The part of the work of CI is supported by the National Natural Science Foundation of China (NNSFC) Grant No. 12205387, No.12475111.

Appendix A: Input and output parameters

The following shows the relationship between the input and output parameters. However, m_3^2 and a_1 remain as input parameters. The index i runs from 1 to 3, and the sum symbol

(\sum_i) is omitted.

$$m_1^2 = \frac{m_3^2 v_2}{v_1} - \frac{\lambda_1 v_1^2}{2} - \frac{\lambda_{345} v_2^2}{2} - \frac{\delta_1 v_S^2}{4}, \quad (\text{A1})$$

$$m_2^2 = \frac{m_3^2 v_1}{v_2} - \frac{\lambda_2 v_2^2}{2} - \frac{\lambda_{345} v_1^2}{2} - \frac{\delta_2 v_S^2}{4}, \quad (\text{A2})$$

$$\lambda_1 = \frac{1}{v_1^2} \left(\sum_{i=1}^3 O_{1i}^2 m_{H_i}^2 - \frac{m_3^2 v_2}{v_1} \right), \quad (\text{A3})$$

$$\lambda_2 = \frac{1}{v_2^2} \left(\sum_{i=1}^3 O_{2i}^2 m_{H_i}^2 - \frac{m_3^2 v_1}{v_2} \right), \quad (\text{A4})$$

$$\lambda_3 = \frac{1}{v_1 v_2} \left(\sum_{i=1}^3 O_{1i} O_{2i} m_{H_i}^2 + m_3^2 \right) - \lambda_4 - \lambda_5, \quad (\text{A5})$$

$$\lambda_4 = \frac{2}{v^2} \left(\frac{m_3^2}{\sin \beta \cos \beta} - m_{H^\pm}^2 \right) - \lambda_5, \quad (\text{A6})$$

$$\lambda_5 = \frac{1}{v^2} \left(\frac{m_3^2}{\sin \beta \cos \beta} - m_A^2 \right), \quad (\text{A7})$$

$$\delta_1 = \frac{2}{v_1 v_S} \sum_{i=1}^3 O_{1i} O_{3i} m_{H_i}^2, \quad (\text{A8})$$

$$\delta_2 = \frac{2}{v_2 v_S} \sum_{i=1}^3 O_{2i} O_{3i} m_{H_i}^2, \quad (\text{A9})$$

$$d_2 = \frac{2}{v_S^2} \left(\frac{\sqrt{2} a_1}{v_S} + \sum_{i=1}^3 O_{3i}^2 m_{H_i}^2 \right), \quad (\text{A10})$$

$$b_2 = \frac{-4\sqrt{2} a_1 - 2b_1 v_S - \delta_1 v_1^2 v_S - \delta_2 v_2^2 v_S - d_2 v_S^3}{2v_S}, \quad (\text{A11})$$

$$b_1 = -m_\chi^2 - \frac{\sqrt{2} a_1}{v_S}. \quad (\text{A12})$$

Appendix B: Trilinear and quartic couplings in the pNG-DM model

We collect trilinear and bilinear couplings of the potential (1) in the gauge eigenstate, which appear in Sec. III.

$$\begin{aligned} C_{\chi\chi h_1} &= \frac{\delta_1}{4} v_1, & C_{\chi\chi h_2} &= \frac{\delta_2}{4} v_2, & C_{\chi\chi s} &= \frac{d_2}{4} v_S, \\ C_{h_1 s} &= \frac{\delta_2}{4} v_1 v_S, & C_{h_2 s} &= \frac{\delta_2}{2} v_2 v_S, & C_{ss} &= \frac{b_1}{2} + \frac{b_2}{2} + \frac{\delta_1}{8} v_1^2 + \frac{\delta_1}{8} v_2^2 + \frac{3d_2}{8} v_S^2. \end{aligned} \quad (\text{B1})$$

-
- [1] J. Aalbers *et al.* (LZ), (2024), [arXiv:2410.17036 \[hep-ex\]](#).
- [2] V. Barger, P. Langacker, M. McCaskey, M. Ramsey-Musolf, and G. Shaughnessy, *Phys. Rev. D* **79**, 015018 (2009), [arXiv:0811.0393 \[hep-ph\]](#).
- [3] C. Gross, O. Lebedev, and T. Toma, *Phys. Rev. Lett.* **119**, 191801 (2017), [arXiv:1708.02253 \[hep-ph\]](#).
- [4] S. Abe, G.-C. Cho, and K. Mawatari, *Phys. Rev. D* **104**, 035023 (2021), [arXiv:2101.04887 \[hep-ph\]](#).
- [5] V. A. Kuzmin, V. A. Rubakov, and M. E. Shaposhnikov, *Phys. Lett.* **155B**, 36 (1985).
- [6] V. A. Rubakov and M. E. Shaposhnikov, *Usp. Fiz. Nauk* **166**, 493 (1996), [*Phys. Usp.*39,461(1996)], [arXiv:hep-ph/9603208 \[hep-ph\]](#).
- [7] K. Funakubo, *Prog. Theor. Phys.* **96**, 475 (1996), [arXiv:hep-ph/9608358 \[hep-ph\]](#).
- [8] A. Riotto, in *Proceedings, Summer School in High-energy physics and cosmology: Trieste, Italy, June 29-July 17, 1998* (1998) pp. 326–436, [arXiv:hep-ph/9807454 \[hep-ph\]](#).
- [9] M. Trodden, *Rev. Mod. Phys.* **71**, 1463 (1999), [arXiv:hep-ph/9803479 \[hep-ph\]](#).
- [10] W. Bernreuther, *Workshop of the Graduate College of Elementary Particle Physics Berlin, Germany, April 2-5, 2001*, *Lect. Notes Phys.* **591**, 237 (2002), [,237(2002)], [arXiv:hep-ph/0205279 \[hep-ph\]](#).
- [11] J. M. Cline, in *Les Houches Summer School - Session 86: Particle Physics and Cosmology: The Fabric of Spacetime Les Houches, France, July 31-August 25, 2006* (2006) [arXiv:hep-ph/0609145 \[hep-ph\]](#).
- [12] D. E. Morrissey and M. J. Ramsey-Musolf, *New J. Phys.* **14**, 125003 (2012), [arXiv:1206.2942 \[hep-ph\]](#).
- [13] T. Konstandin, *Phys. Usp.* **56**, 747 (2013), [*Usp. Fiz. Nauk*183,785(2013)], [arXiv:1302.6713 \[hep-ph\]](#).
- [14] E. Senaha, *Symmetry* **12**, 733 (2020).
- [15] K. Kajantie, M. Laine, K. Rummukainen, and M. E. Shaposhnikov, *Phys. Rev. Lett.* **77**, 2887 (1996), [arXiv:hep-ph/9605288](#).
- [16] K. Rummukainen, M. Tsy-pin, K. Kajantie, M. Laine, and M. E. Shaposhnikov, *Nucl. Phys. B* **532**, 283 (1998), [arXiv:hep-lat/9805013](#).

- [17] F. Csikor, Z. Fodor, and J. Heitger, *Phys. Rev. Lett.* **82**, 21 (1999), [arXiv:hep-ph/9809291](#).
- [18] Y. Aoki, F. Csikor, Z. Fodor, and A. Ukawa, *Phys. Rev. D* **60**, 013001 (1999), [arXiv:hep-lat/9901021](#).
- [19] G.-C. Cho, C. Idegawa, and E. Senaha, *Phys. Lett. B* **823**, 136787 (2021), [arXiv:2105.11830 \[hep-ph\]](#).
- [20] N. Aghanim *et al.* (Planck), *Astron. Astrophys.* **641**, A6 (2020), [Erratum: *Astron. Astrophys.* 652, C4 (2021)], [arXiv:1807.06209 \[astro-ph.CO\]](#).
- [21] X.-M. Jiang, C. Cai, Z.-H. Yu, Y.-P. Zeng, and H.-H. Zhang, *Phys. Rev. D* **100**, 075011 (2019), [arXiv:1907.09684 \[hep-ph\]](#).
- [22] Z. Zhang, C. Cai, X.-M. Jiang, Y.-L. Tang, Z.-H. Yu, and H.-H. Zhang, *JHEP* **05**, 160 (2021), [arXiv:2102.01588 \[hep-ph\]](#).
- [23] T. Biekötter and M. O. Olea-Romacho, *JHEP* **10**, 215 (2021), [arXiv:2108.10864 \[hep-ph\]](#).
- [24] T. Biekötter, P. Gabriel, M. O. Olea-Romacho, and R. Santos, *JHEP* **10**, 126 (2022), [arXiv:2207.04973 \[hep-ph\]](#).
- [25] G.-C. Cho, C. Idegawa, and R. Inumiya, *Nucl. Phys. B* **1007**, 116688 (2024), [arXiv:2312.05776 \[hep-ph\]](#).
- [26] G. C. Branco, P. M. Ferreira, L. Lavoura, M. N. Rebelo, M. Sher, and J. P. Silva, *Phys. Rept.* **516**, 1 (2012), [arXiv:1106.0034 \[hep-ph\]](#).
- [27] G.-C. Cho and C. Idegawa, *Nucl. Phys. B* **994**, 116320 (2023), [arXiv:2304.10096 \[hep-ph\]](#).
- [28] P. B. Arnold and L. D. McLerran, *Phys. Rev. D* **36**, 581 (1987).
- [29] A. I. Bochkarev and M. E. Shaposhnikov, *Mod. Phys. Lett. A* **2**, 417 (1987).
- [30] K. Funakubo and E. Senaha, *Phys. Rev. D* **79**, 115024 (2009), [arXiv:0905.2022 \[hep-ph\]](#).
- [31] E. J. Weinberg, *Radiative corrections as the origin of spontaneous symmetry breaking*, Ph.D. thesis, Harvard U. (1973), [arXiv:hep-th/0507214](#).
- [32] R. Jackiw, *Phys. Rev. D* **9**, 1686 (1974).
- [33] L. Dolan and R. Jackiw, *Phys. Rev. D* **9**, 3320 (1974).
- [34] R. R. Parwani, *Phys. Rev. D* **45**, 4695 (1992), [Erratum: *Phys. Rev. D* 48, 5965 (1993)], [arXiv:hep-ph/9204216](#).
- [35] S. Nie and M. Sher, *Phys. Lett. B* **449**, 89 (1999), [arXiv:hep-ph/9811234](#).
- [36] S. Kanemura, T. Kasai, and Y. Okada, *Phys. Lett. B* **471**, 182 (1999), [arXiv:hep-ph/9903289](#).

- [37] C.-Y. Chen, S. Dawson, and I. M. Lewis, *Phys. Rev. D* **91**, 035015 (2015), [arXiv:1410.5488 \[hep-ph\]](#).
- [38] A. G. Akeroyd, A. Arhrib, and E.-M. Naimi, *Phys. Lett. B* **490**, 119 (2000), [arXiv:hep-ph/0006035](#).
- [39] M. Aoki, T. Komatsu, and H. Shibuya, *PTEP* **2022**, 063B05 (2022), [arXiv:2106.03439 \[hep-ph\]](#).
- [40] N. Chen, T. Li, and Y. Wu, *JHEP* **08**, 117 (2020), [arXiv:2004.10148 \[hep-ph\]](#).
- [41] H. E. Haber and D. O’Neil, *Phys. Rev. D* **83**, 055017 (2011), [arXiv:1011.6188 \[hep-ph\]](#).
- [42] J. Haller, A. Hoecker, R. Kogler, K. Mönig, T. Peiffer, and J. Stelzer, *Eur. Phys. J. C* **78**, 675 (2018), [arXiv:1803.01853 \[hep-ph\]](#).
- [43] C. L. Wainwright, *Comput. Phys. Commun.* **183**, 2006 (2012), [arXiv:1109.4189 \[hep-ph\]](#).
- [44] G. Belanger, F. Boudjema, A. Pukhov, and A. Semenov, *Nuovo Cim. C* **033N2**, 111 (2010), [arXiv:1005.4133 \[hep-ph\]](#).
- [45] G. Belanger, A. Mjallal, and A. Pukhov, *Eur. Phys. J. C* **81**, 239 (2021), [arXiv:2003.08621 \[hep-ph\]](#).
- [46] C. A. J. O’Hare, *Phys. Rev. Lett.* **127**, 251802 (2021), [arXiv:2109.03116 \[hep-ph\]](#).
- [47] S. Kanemura, Y. Okada, and E. Senaha, *Phys. Lett. B* **606**, 361 (2005), [arXiv:hep-ph/0411354](#).
- [48] C. Grojean, G. Servant, and J. D. Wells, *Phys. Rev. D* **71**, 036001 (2005), [arXiv:hep-ph/0407019](#).
- [49] V. Shiltsev, in *17th Conference on Flavor Physics and CP Violation* (2019) [arXiv:1907.01545 \[physics.acc-ph\]](#).